Electronic Supplementary Information

For the Manuscript Entitled

Heterometallic coordination polymers: Syntheses, structures and heterogeneous catalytic applications

Deepak Bansal,[†] Saurabh Pandey,[†] Geeta Hundal,[‡] Rajeev Gupta[†]*

[†]Department of Chemistry, University of Delhi, Delhi – 110 007 and [‡]Department of Chemistry, Guru Nanak Dev University, Amritsar, Punjab – 143 005

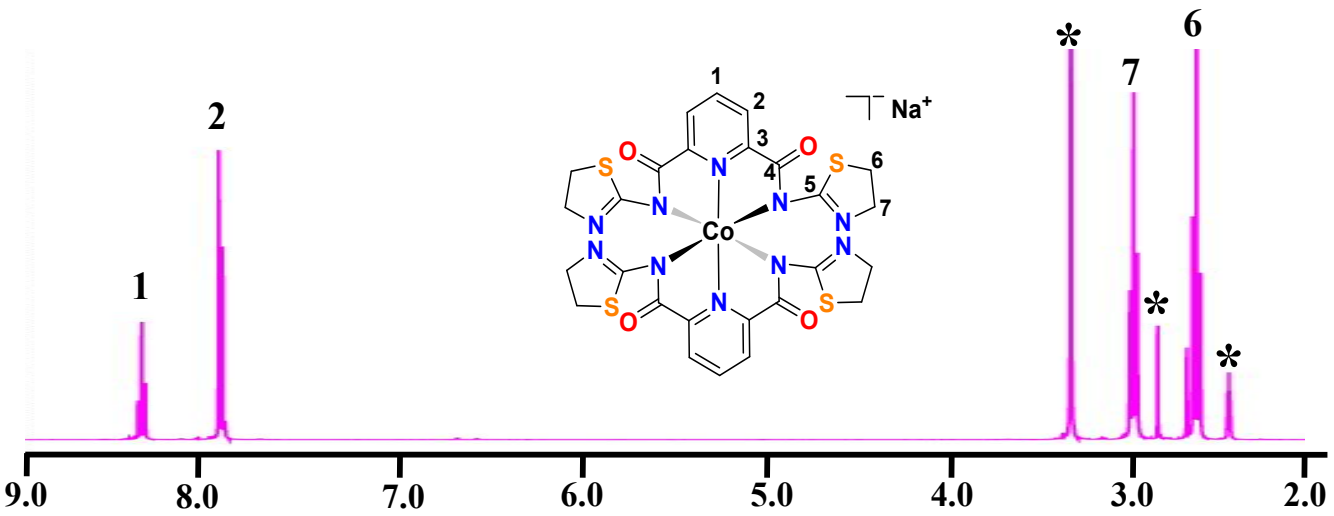

Figure S1. ^{1}H NMR spectrum of metalloligand **1** in d_6-DMSO solvent.* representsthe residual solvent and/or adventitious water peaks.

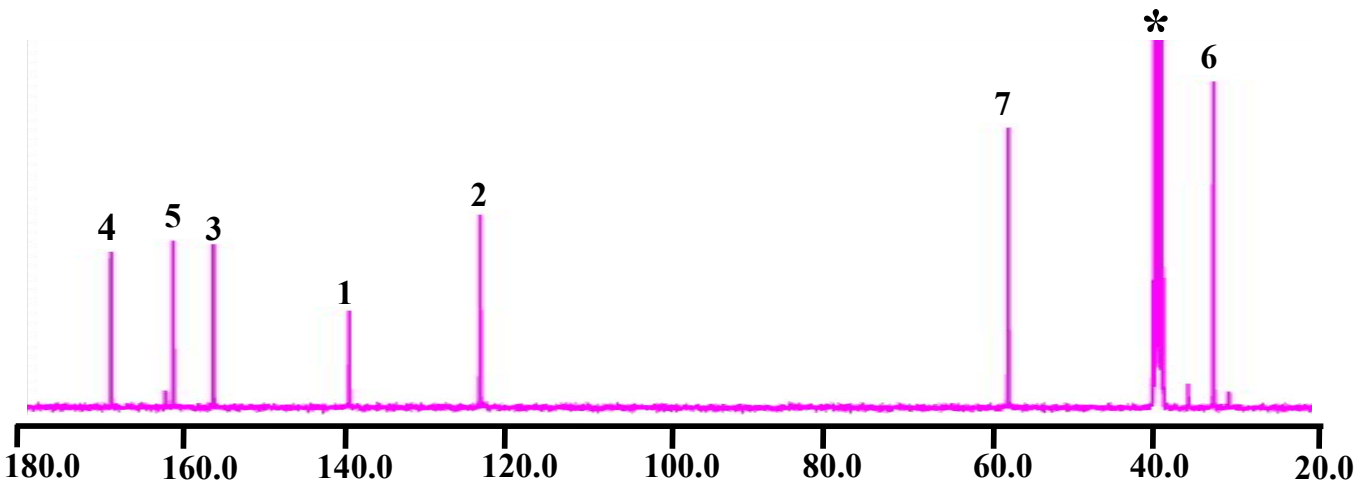

Figure S2. ^{13}C NMR spectrum of metalloligand **1** in d_6-DMSO solvent**.** * representsthe residual solvent peak.

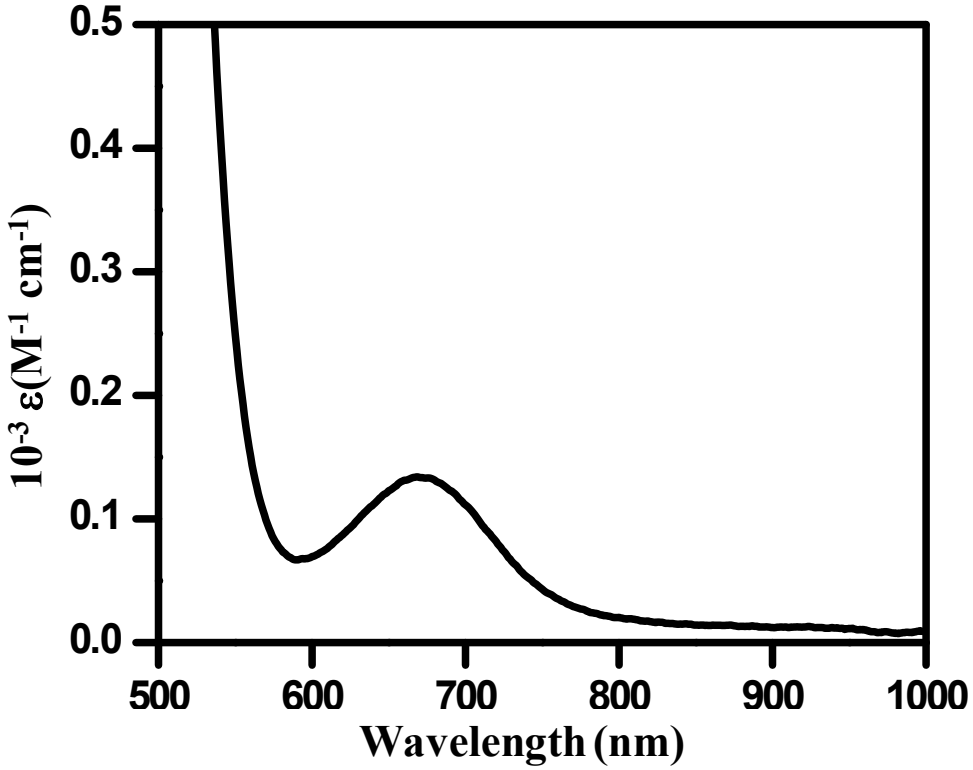

Figure S3. UV-Visible spectrumof metalloligand **1** in DMF solvent.

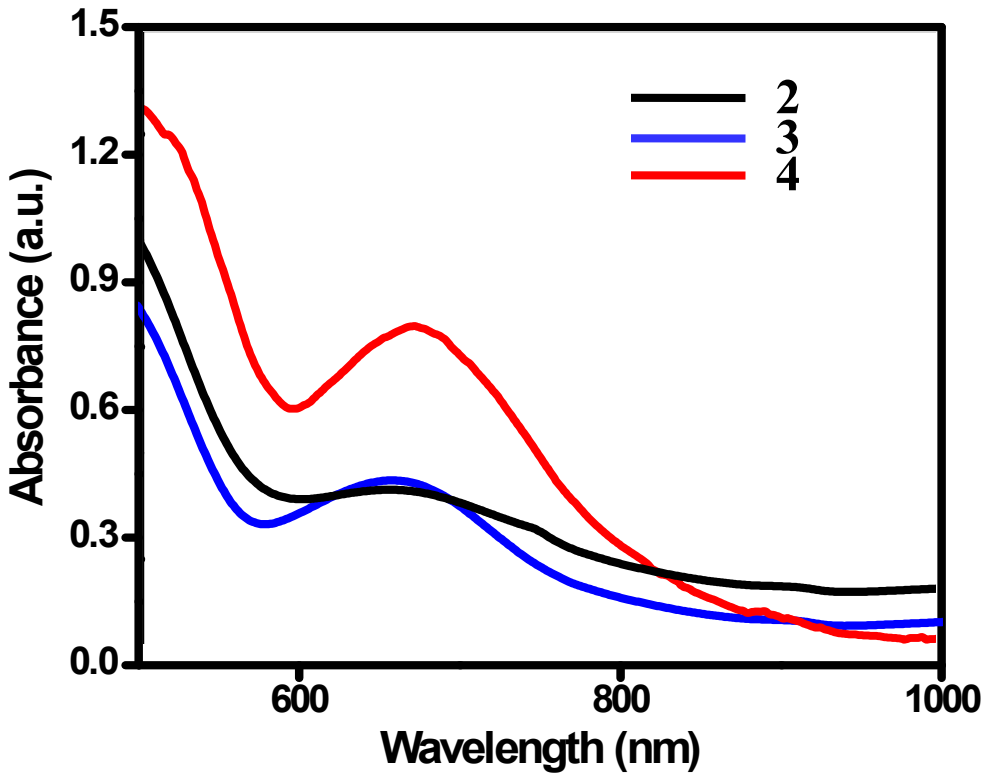

Figure S4. Diffused reflectance absorption spectra for HCPs **2 – 4**.

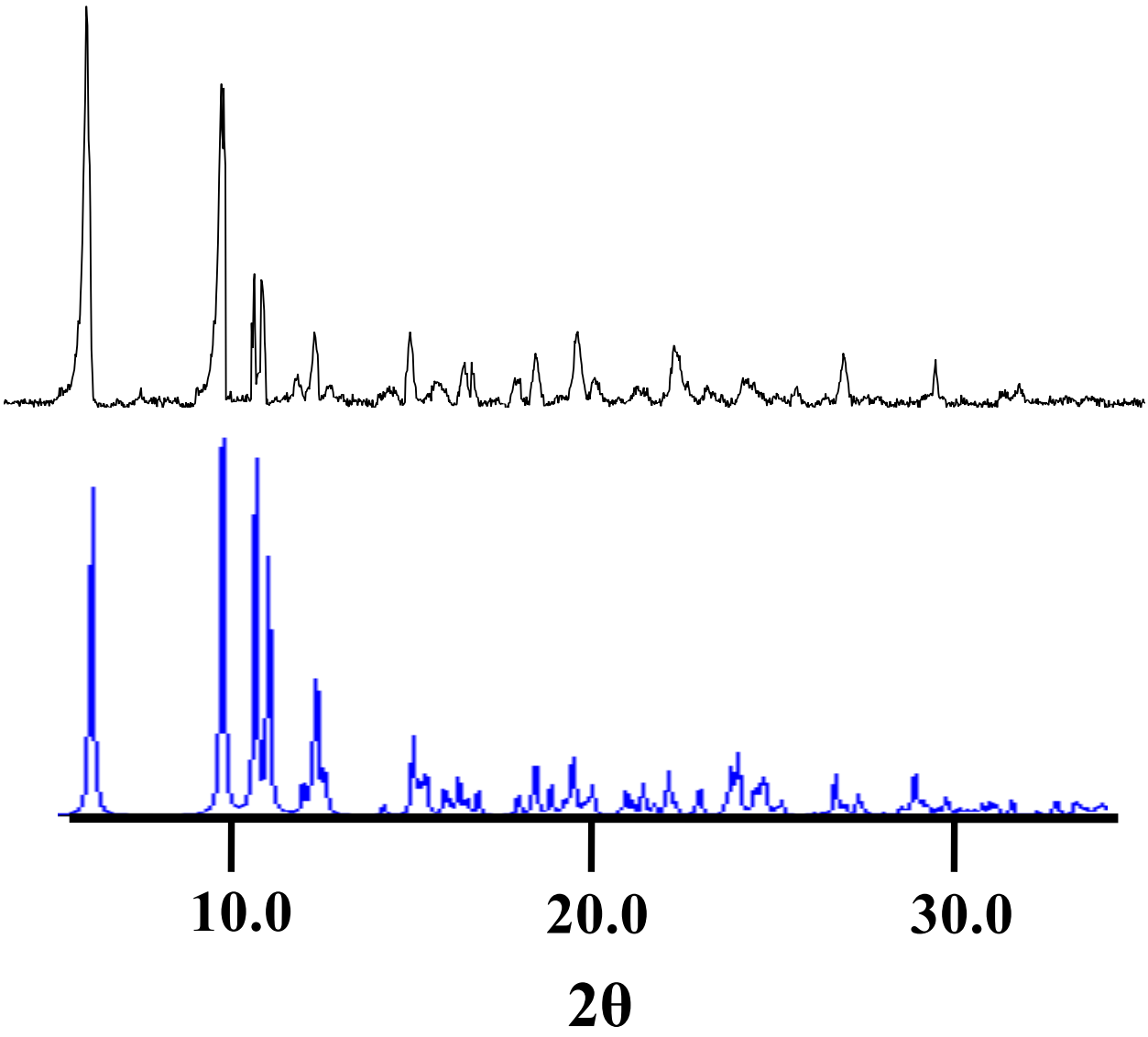

Figure S5. XRPD pattern for HCP **2**; as synthesized (black trace) and the one simulated from the single crystal structure analysis (lower) using Mercury 3.4.

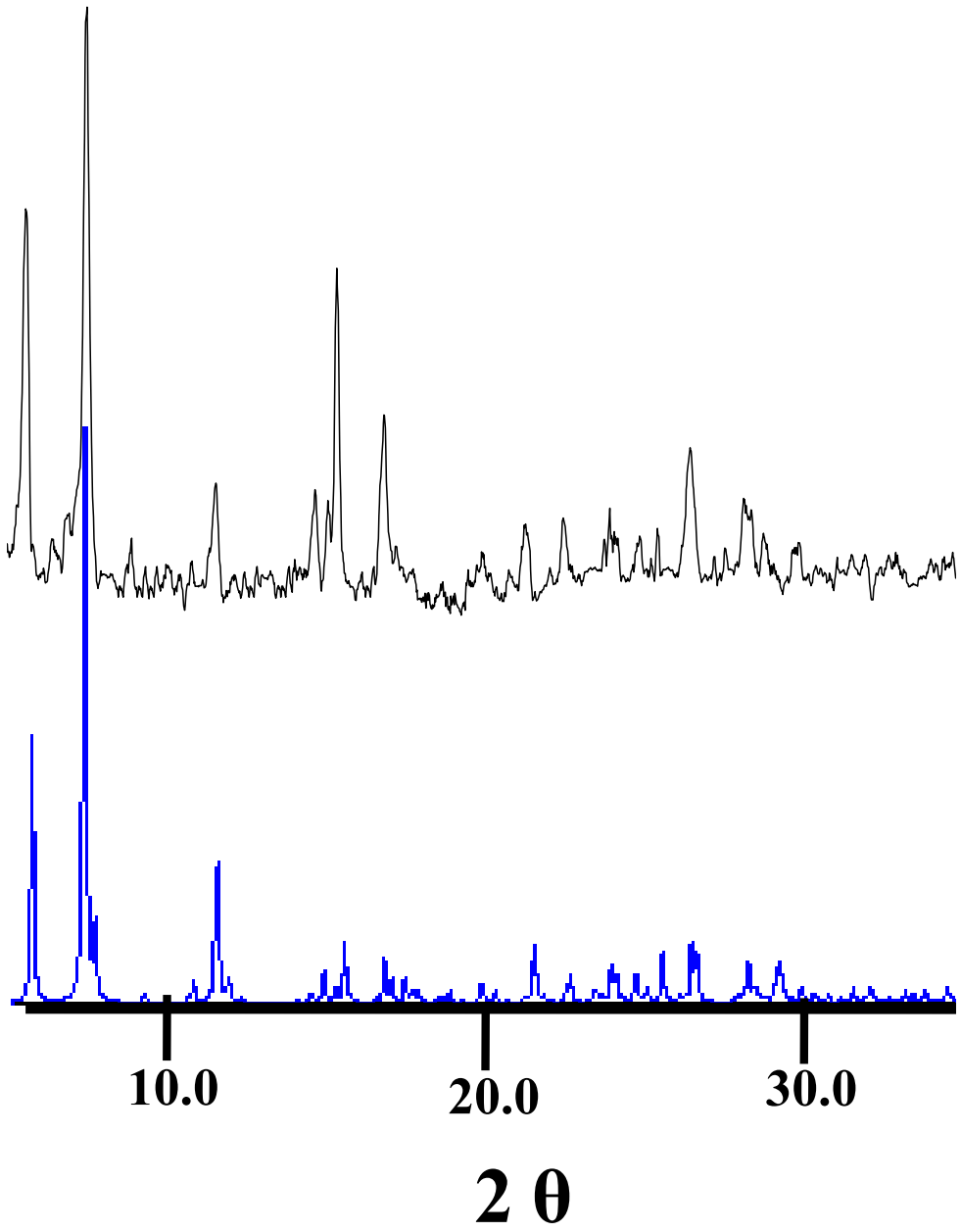

Figure S6. XRPD pattern for HCP **3**; as synthesized (black trace) and the one simulated from the single crystal structure analysis (lower) using Mercury 3.4.

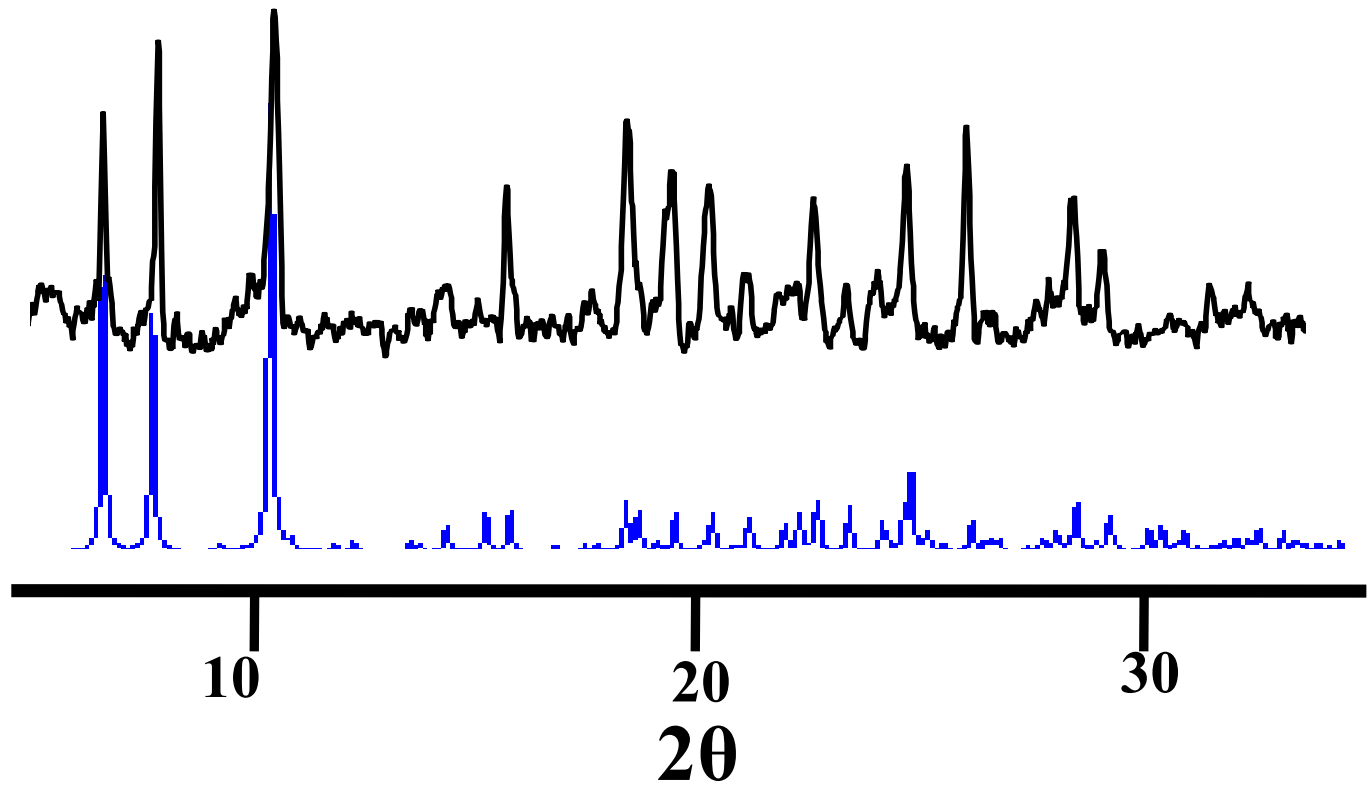

Figure S7. XRPD pattern for HCP **4**; as synthesized (black trace) and the one simulated from the single crystal structure analysis (lower) using Mercury 3.4.

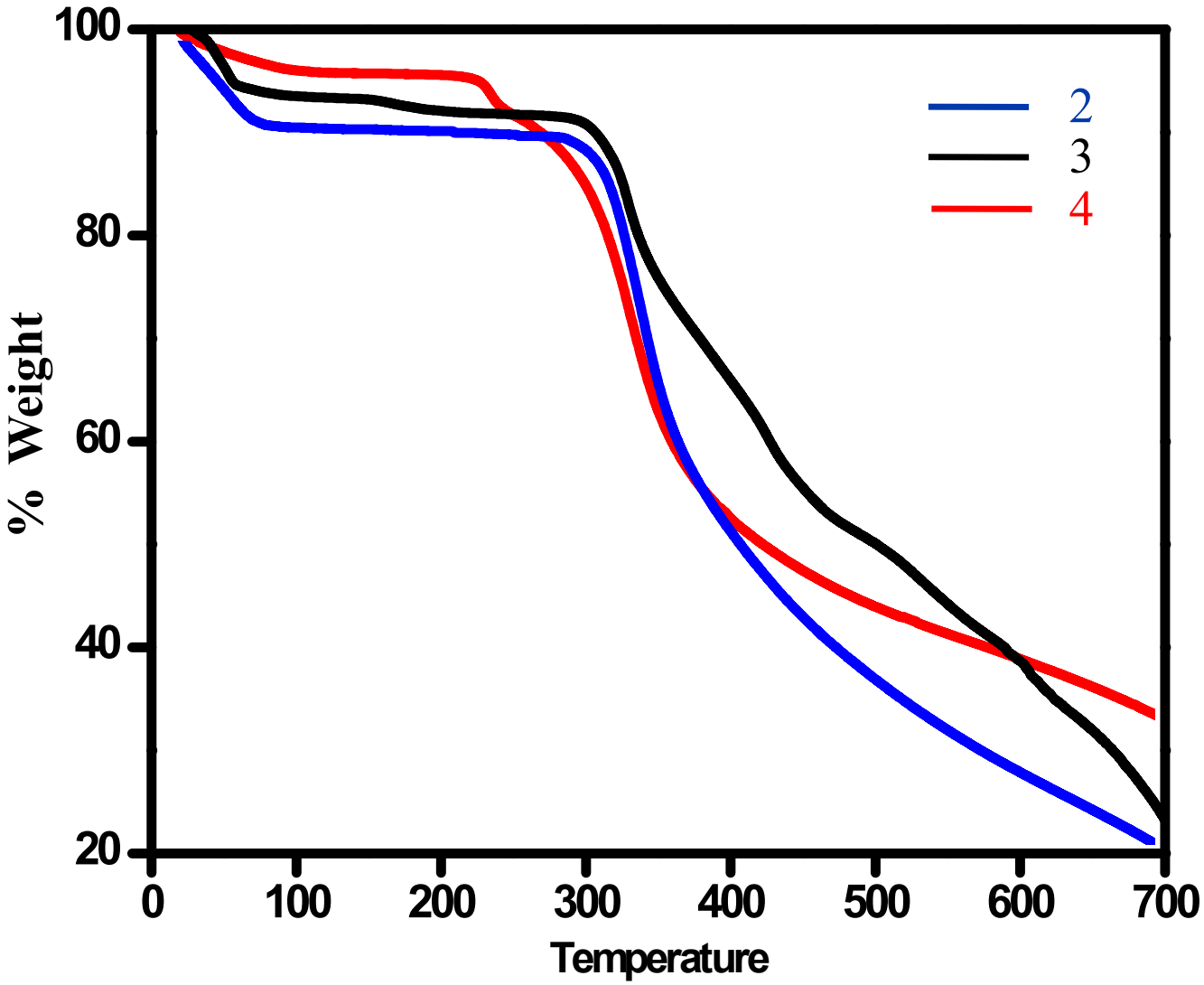

Figure S8. Thermal Gravimetric Analysis (TGA)profiles for HCPs **2 – 4**.

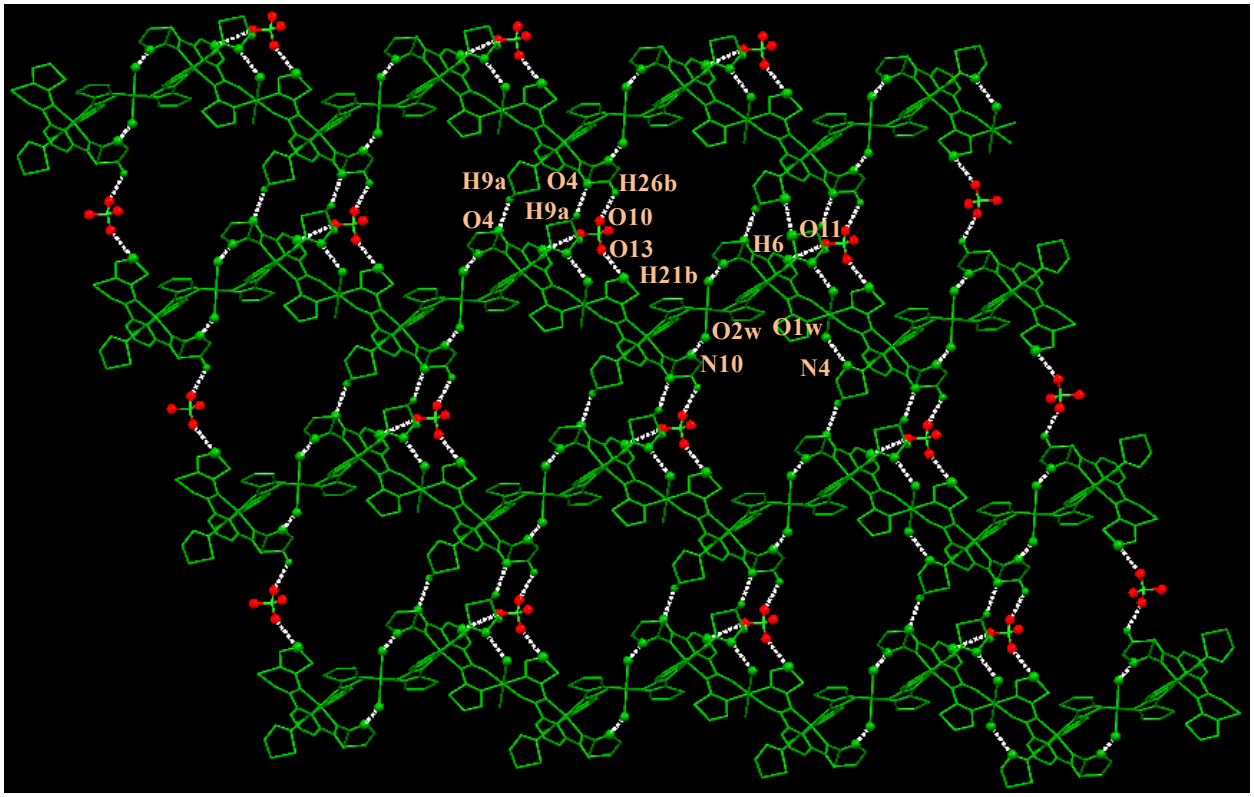

Figure S9. Solid-state packing diagram of HCP **2** in a view along *b*-axis.

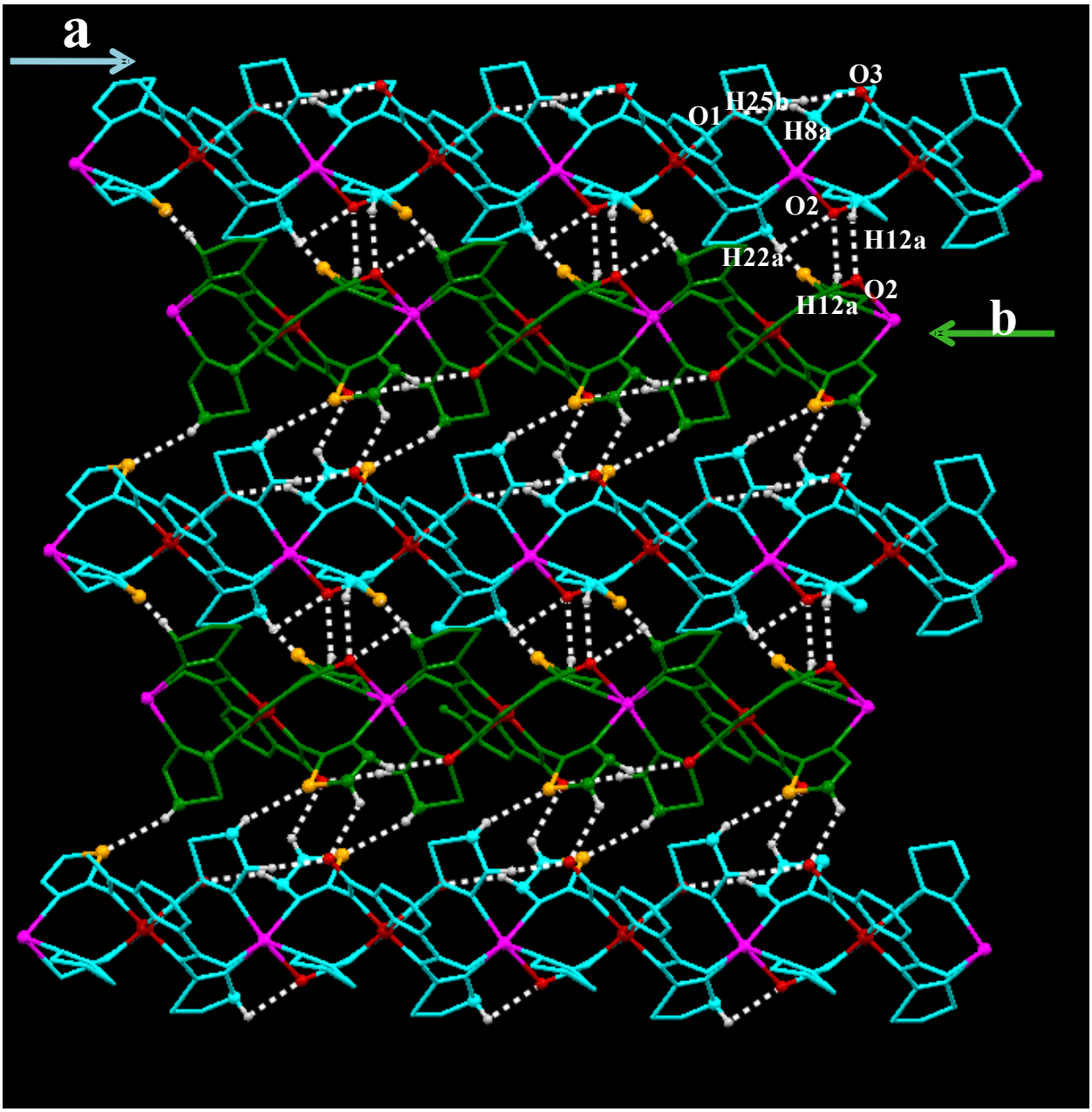

Figure S10. Weak interactions in HCP **3** exhibiting 2D sheet formation from 1D chains.

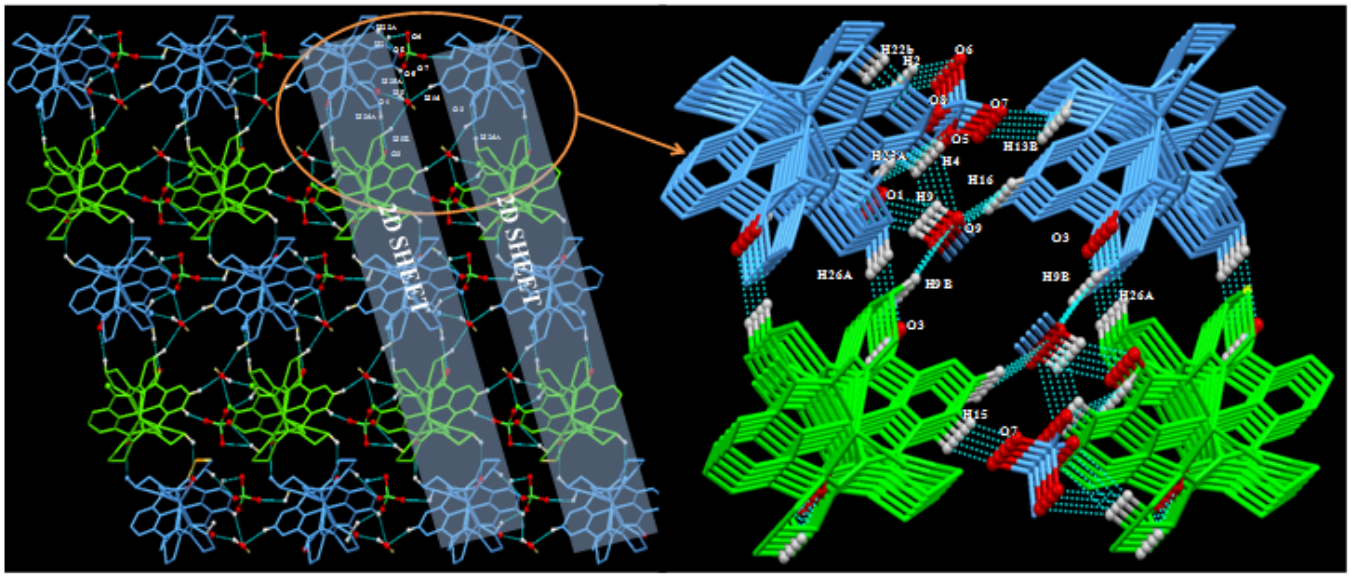

Figure S11. Solid-state packing diagram of HCP **3** in an offset top view along the *a*-axis.

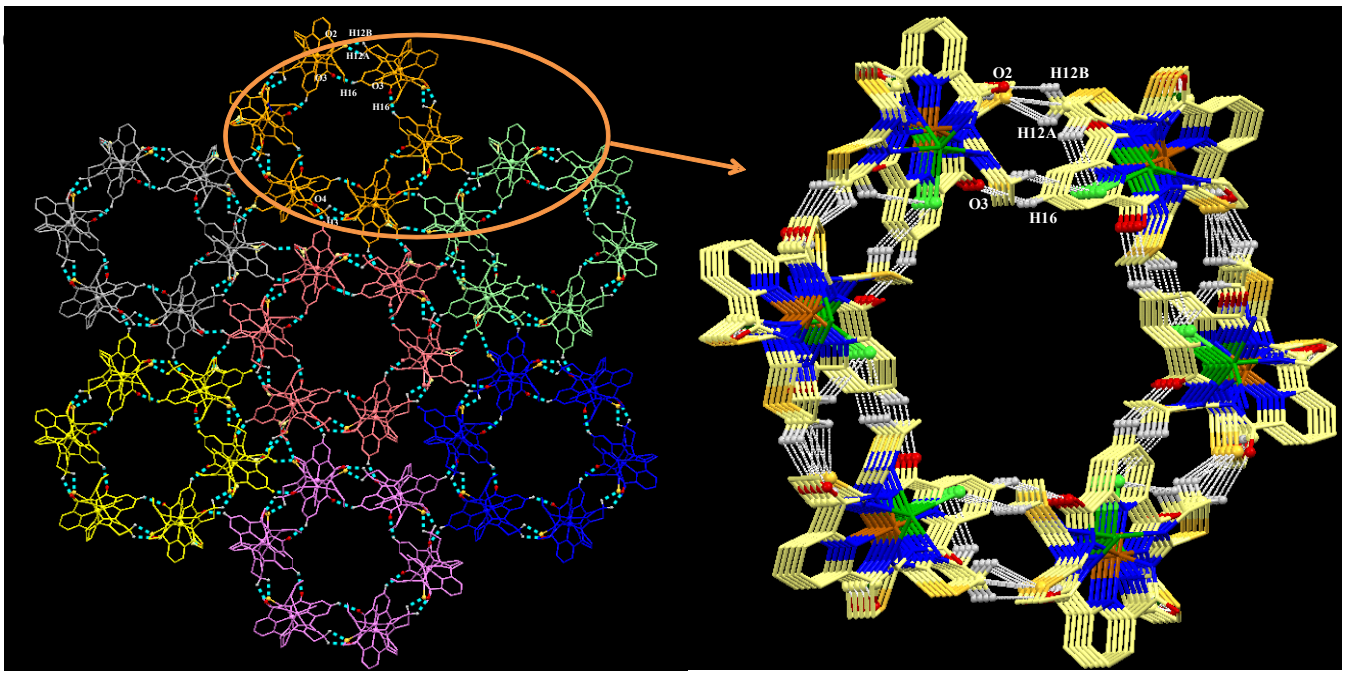

Figure S12. Top view along the *c*-axis and an enlarged view representing inward growth of HCP **4**.

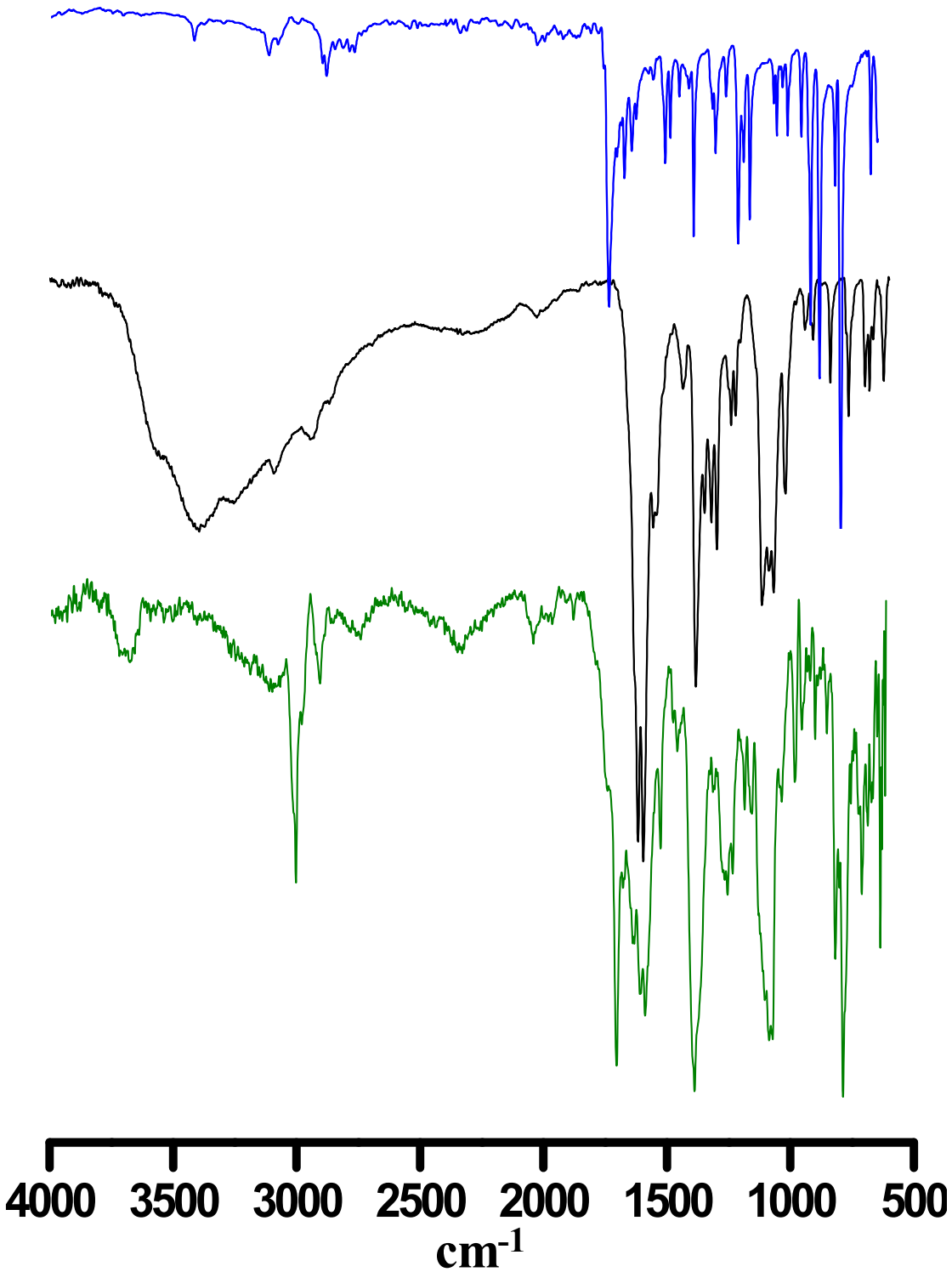

Figure S13.Comparative FTIR spectra of benzaldehyde (blue trace), HCP **2** (black trace) and impregnated crystals of HCP **2** in CH_2Cl_2containing benzaldehyde. The $\nu_{C=O}$ stretch for neat benzaldehyde was observed at 1705cm^{-1} while shifted to ca. 1690 cm^{-1} after treatment with HCP **2**.

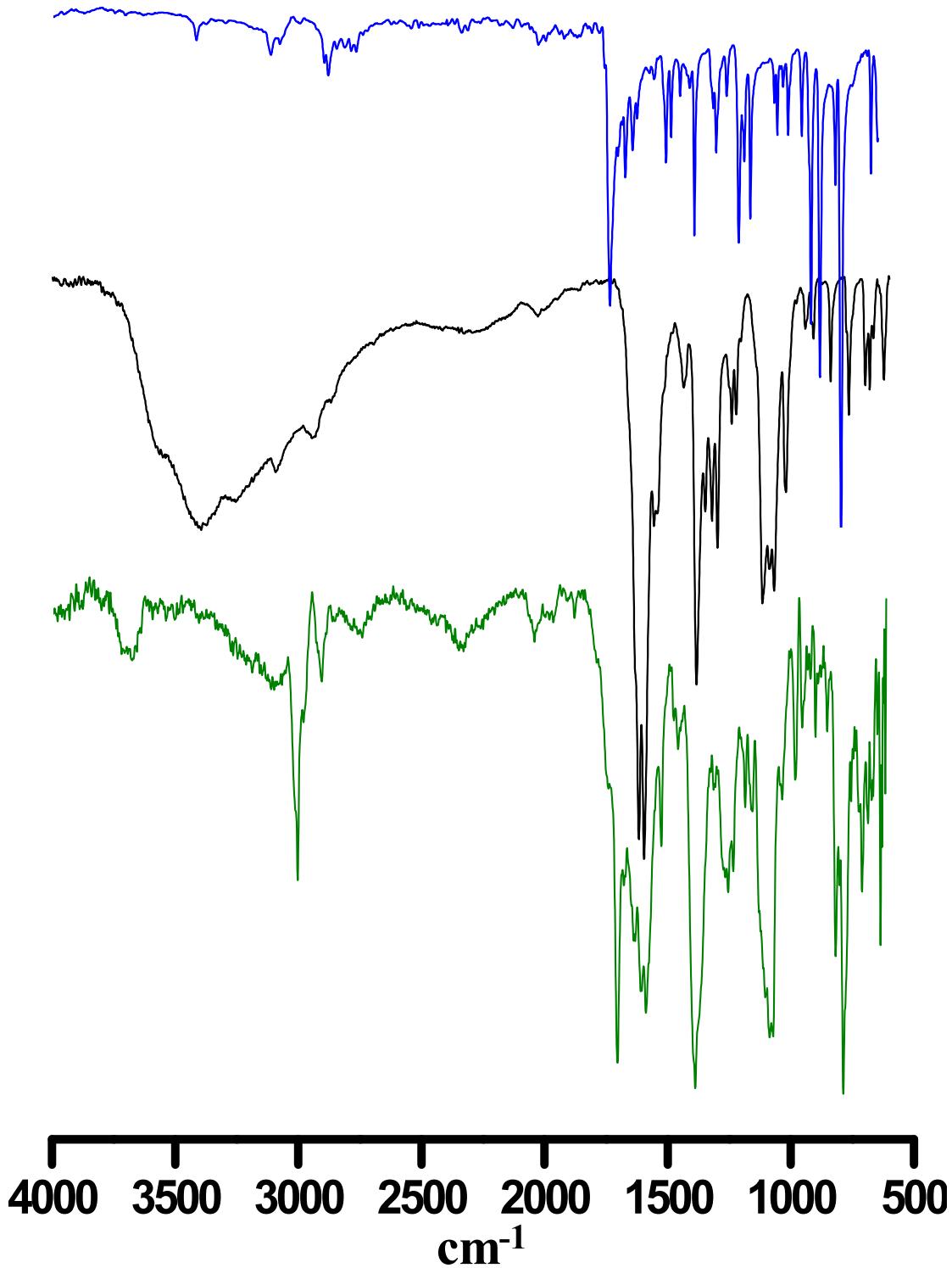

Figure S14.Comparative FTIR spectra of 1-naphthaldehyde (blue trace), HCP **2** (black trace) and impregnated crystals of HCP **2** in CH_2Cl_2 containing 1-naphthaldehyde. The $\nu_{C=O}$ stretch for neat 1-naphthaldehyde was observed at 1702 cm^{-1} while shifted to ca. 1690 cm^{-1} after treatment with HCP **2**.

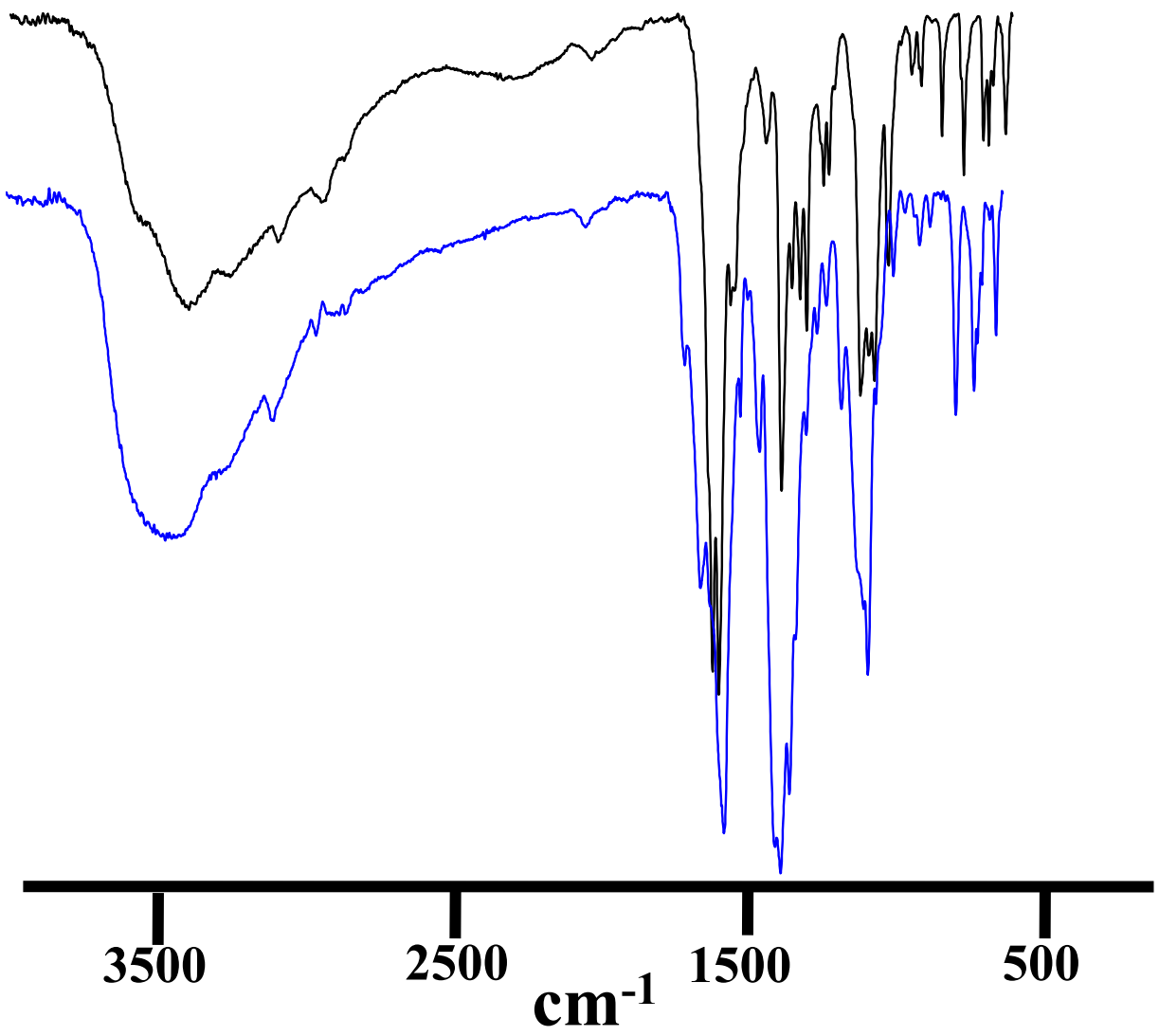

Figure S15. FTIR spectra for HCP **2**; before (black trace) and after the Knoevenagel condensation reaction of benzaldehyde with malononitrile (blue trace).

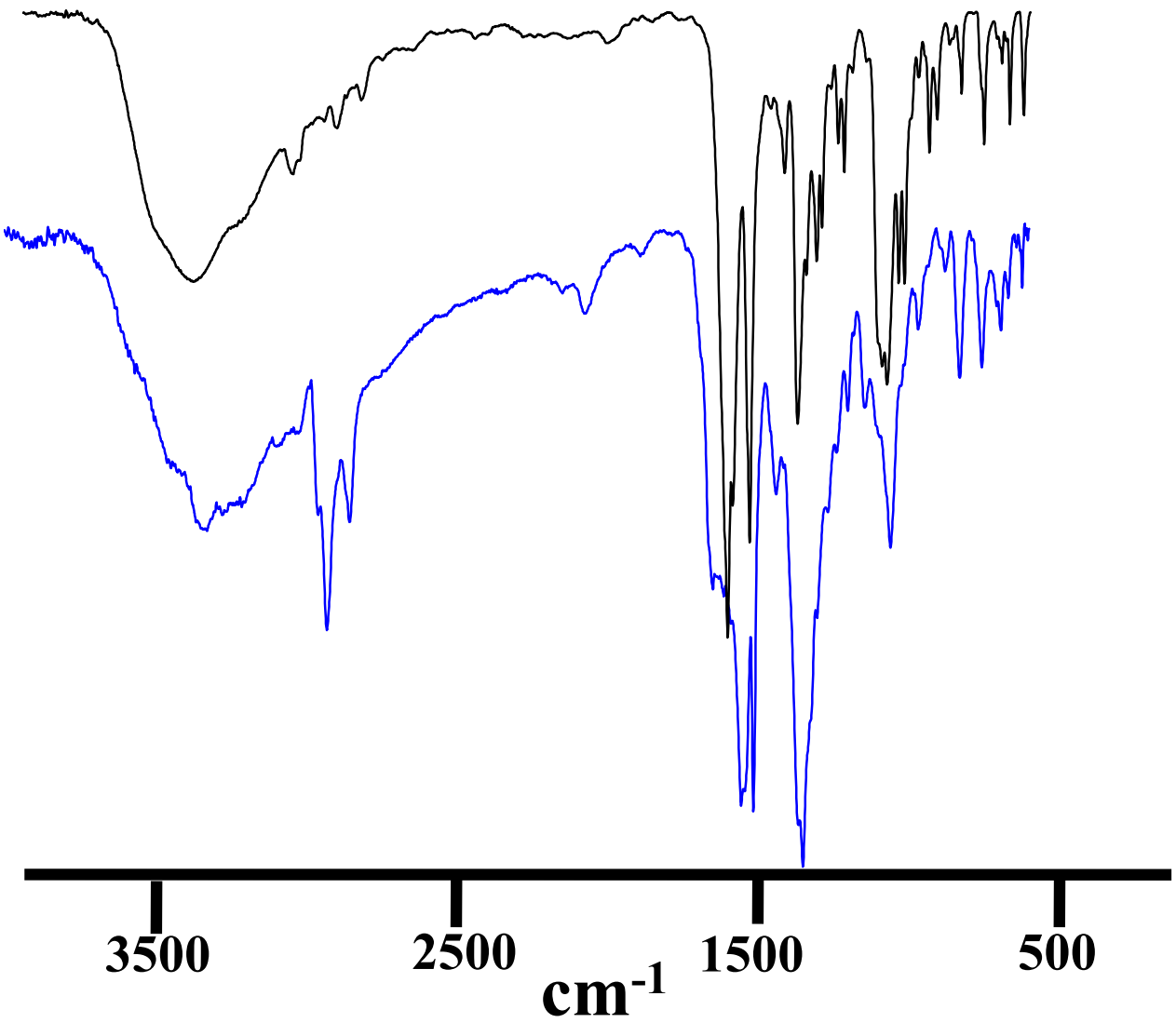

Figure S16. FTIR spectra for HCP **3**; before (black trace) and after the Knoevenagel condensation reaction of benzaldehyde with malononitrile (blue trace).

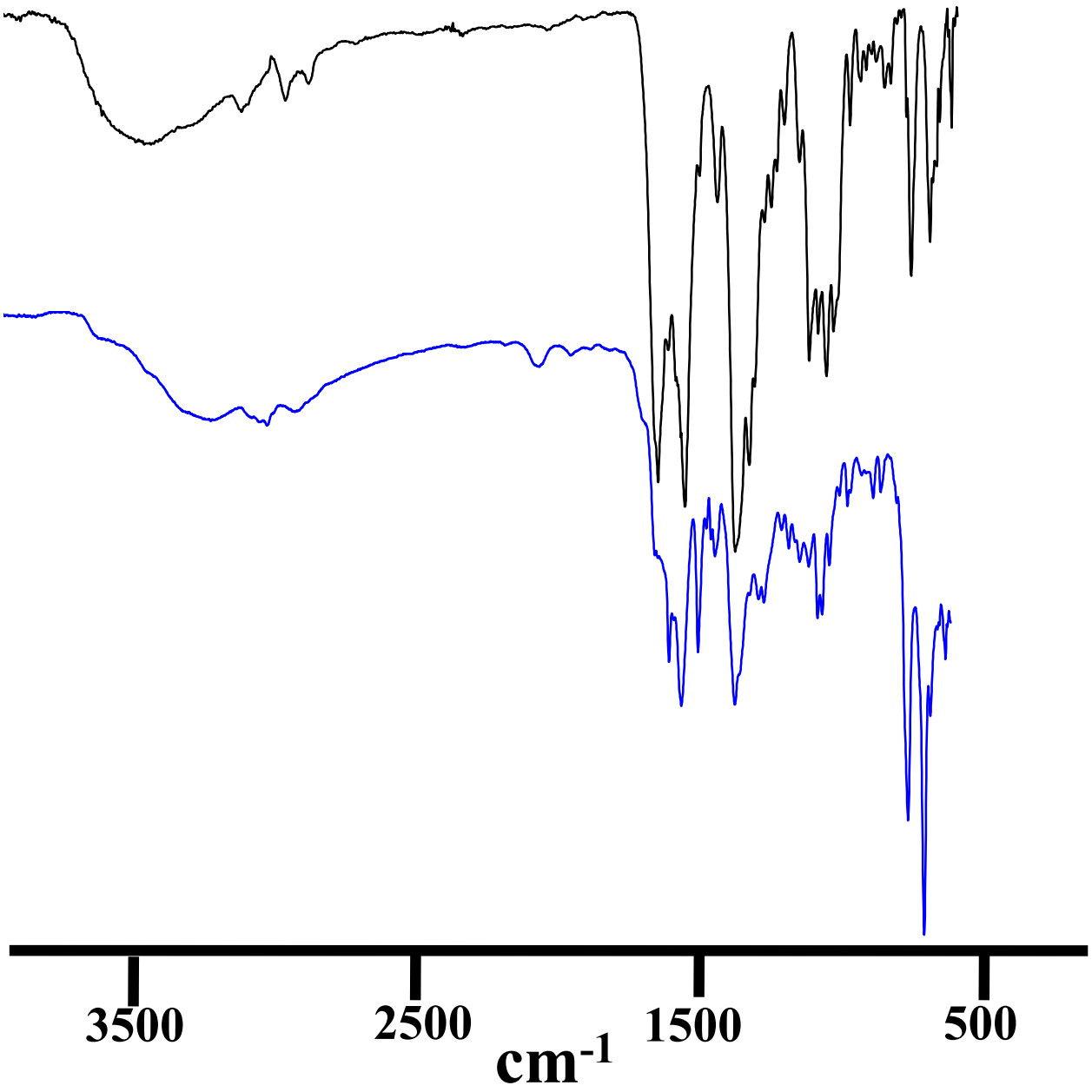

Figure S17. FTIR spectra for HCP **4**; before (black trace) and after the Knoevenagel condensation reaction of benzaldehyde with malononitrile (blue trace).

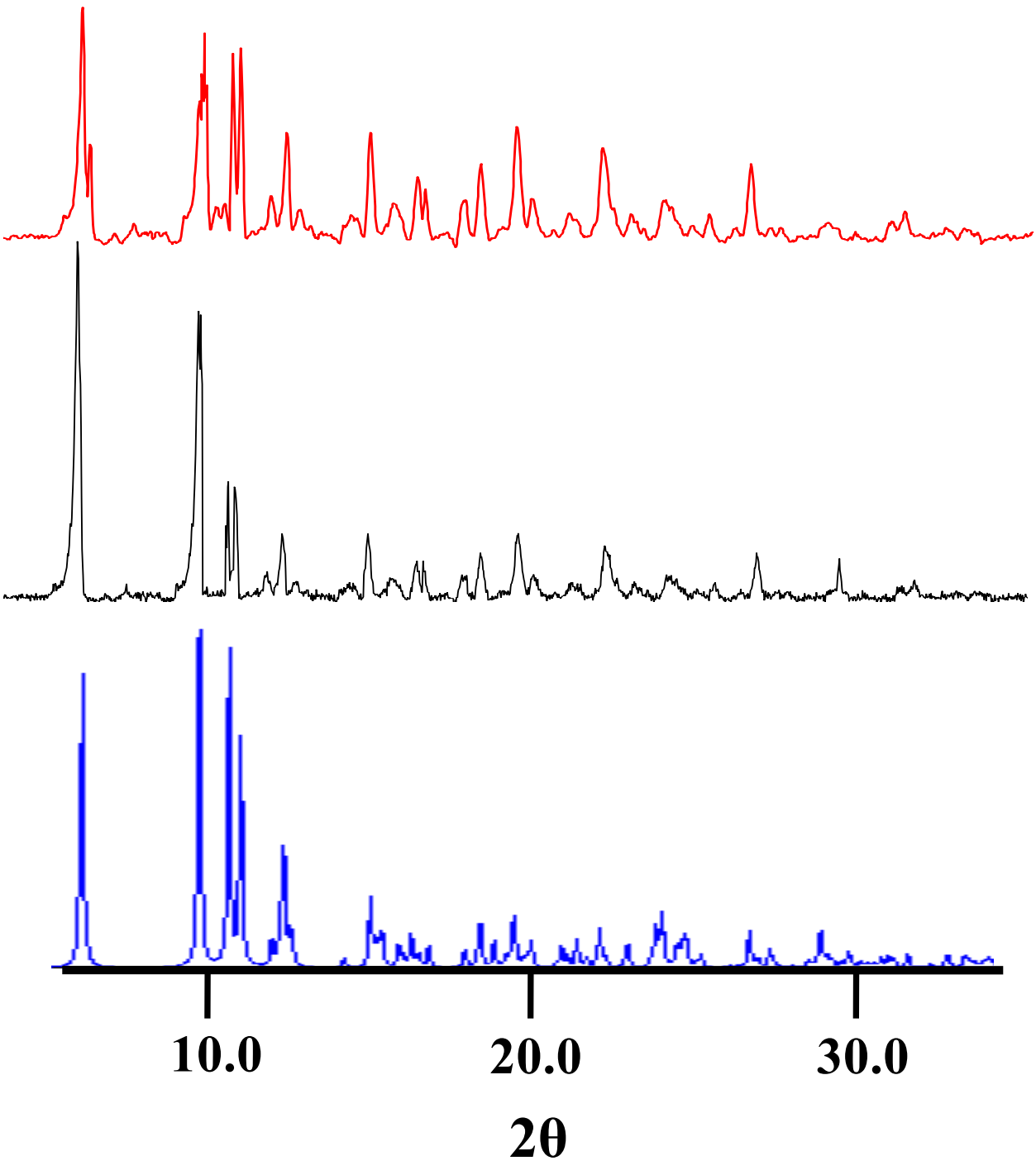

Figure S18. XRPD pattern for HCP **2**before (black trace) and after the Knoevenagel condensation reaction of benzaldehyde with malononitrile (red trace) and comparison with the simulated one from the single crystal structure analysis (blue trace) using Mercury 3.4.

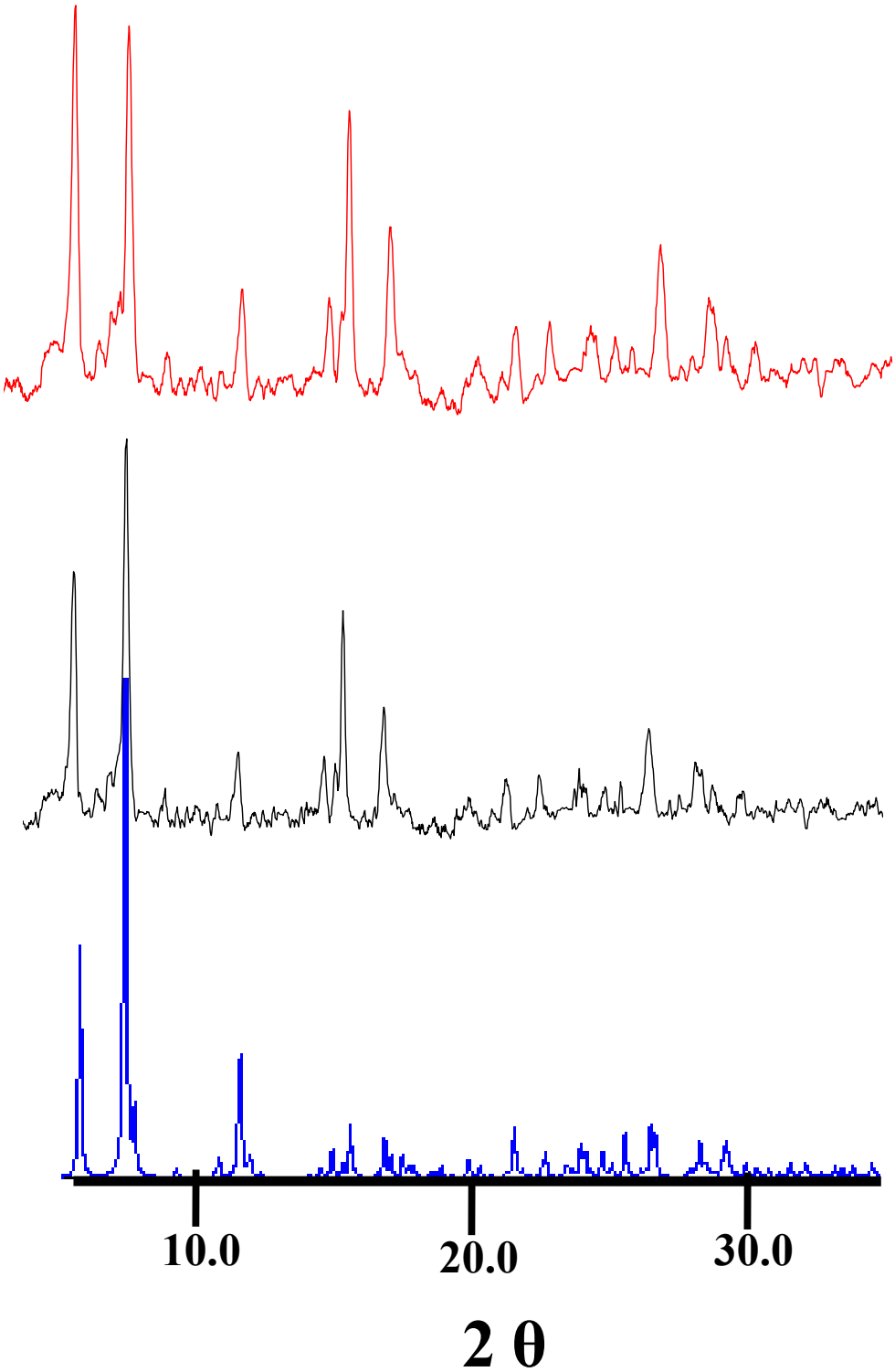

Figure S19. XRPD pattern for HCP **3**before (black trace) and after the Knoevenagel condensation reaction of benzaldehyde with malononitrile (red trace) and comparison with the simulated one from the single crystal structure analysis (blue trace) using Mercury 3.4.

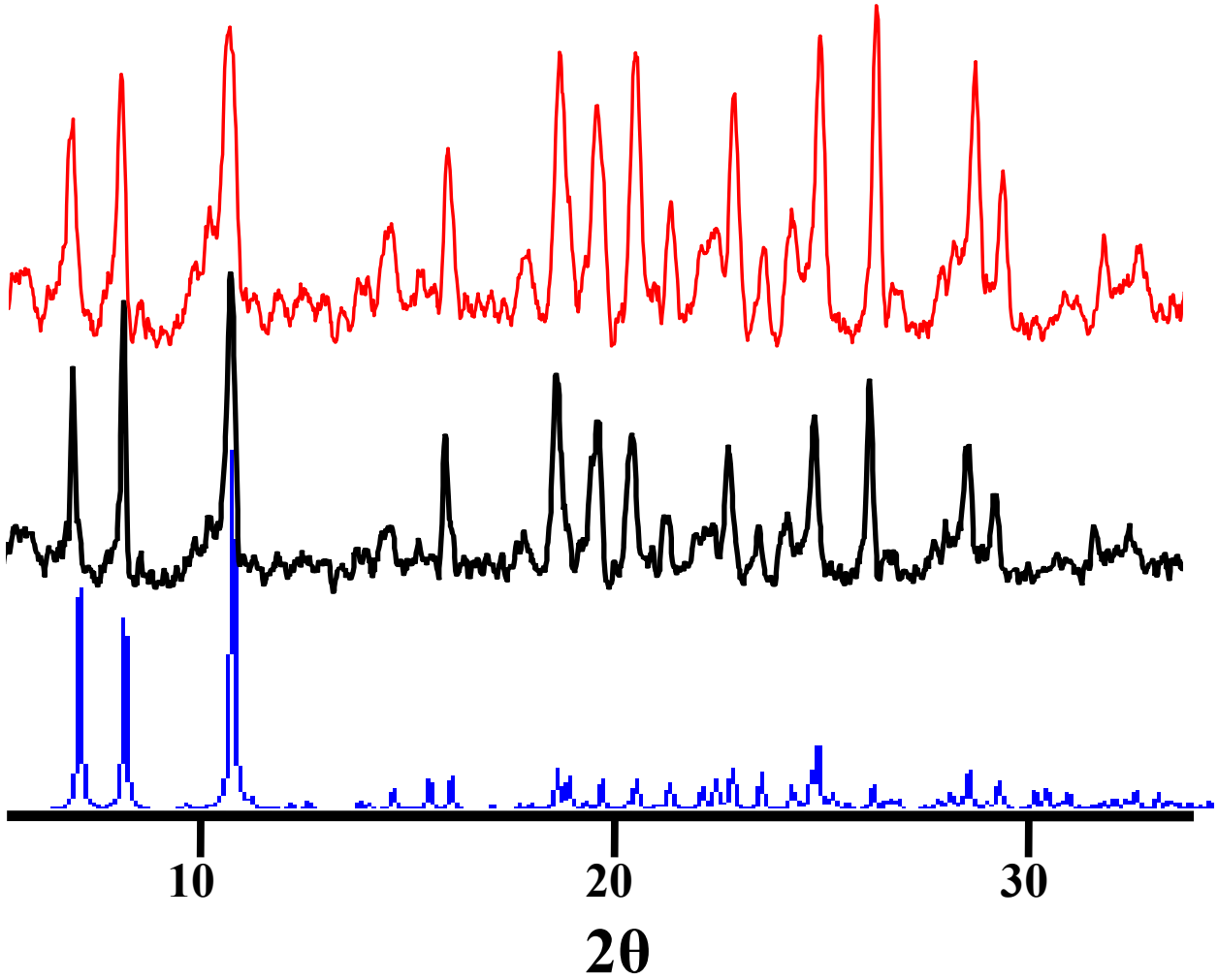

Figure S20. XRPD pattern for HCP **4**before (black trace) and after the Knoevenagel condensation reaction of benzaldehyde with malononitrile (red trace)and comparison with the simulated one from the single crystal structure analysis (blue trace) using Mercury 3.4.

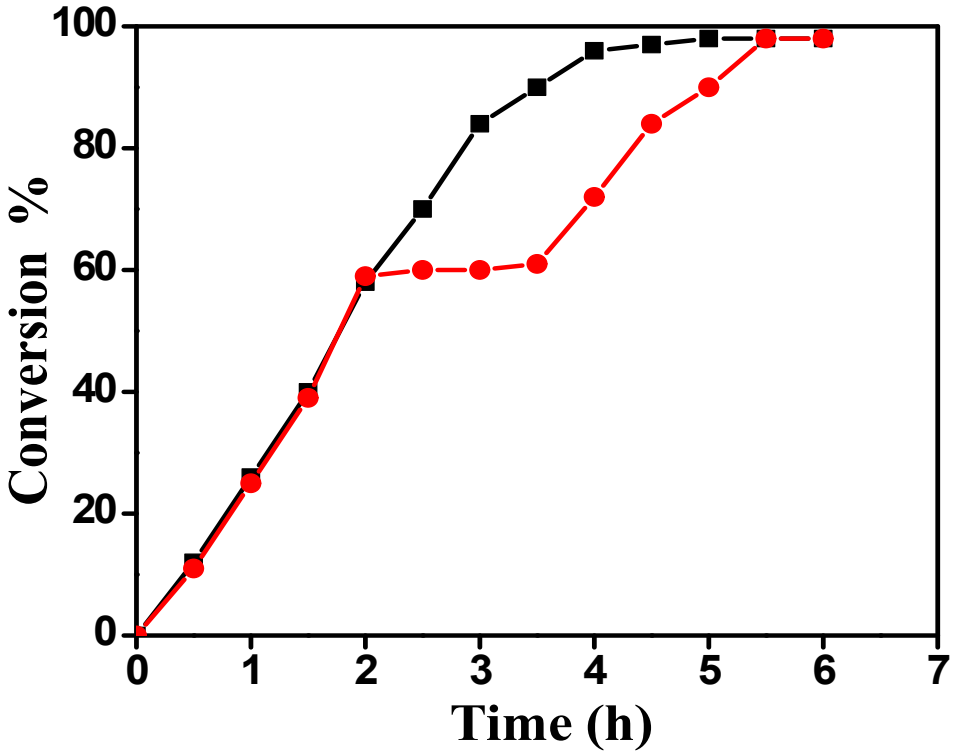

Figure S21. KCR of benzaldehyde with malononitrile in presence of HCP **2** displaying the maximum conversion at ca. 4 h (shown in black squares). Removal of HCP **2** at 2 h led to the cease of catalysis while re-adding results in re-start of the reaction (shown in red spheres).

Table S1. Selected bond lengths (Å) and bond angles (°) for complex **1**and HCP**2**.

Bond	1[a]	Bond	2	Bond	2
Co-N1	1.957(3)	Co-N1	2.013(5)	O1-Zn1	2.113(4)
Co-N2	1.880(3)	Co-N2	1.869(5)	O3-Zn2	2.077(4)
Co-N3	1.951(3)	Co-N3	1.945(5)	O1W-Zn2	2.181(5)
N2-Co-N2$^{\#1}$	178.1(2)	Co-N6	1.952(5)	O2W-Zn1	2.153(5)
N1-Co-N3	161.65(15)	Co-N7	1.875(5)	N5-Zn1-N5$^{\#1}$	180.0
N2-Co-N3	81.05(15)	Co-N8	2.043(5)	N5-Zn1-O1	82.61(18)
N1-Co-N2$^{\#1}$	100.71(15)	N2-Co-N7	171.9(2)	N5$^{\#1}$-Zn1-O1	97.40(18)
N1-Co-N2	80.62(15)	N2-Co-N3	80.6(2)	N5-Zn1-O1$^{\#1}$	97.39(18)
N2$^{\#1}$-Co-N3	97.64(15)	N7-Co-N3	95.2(2)	N5$^{\#1}$-Zn1-O1$^{\#1}$	82.60(18)
N3-Co-N3$^{\#1}$	91.4(2)	N2-Co-N6	92.7(3)	O1-Zn1-O1$^{\#1}$	179.998(2)
N3-Co-N1$^{\#1}$	91.88(15)	N7-Co-N6	80.6(2)	N5-Zn1-O2W	90.3(2)
N1-Co-N1$^{\#1}$	90.7(2)	N3-Co-N6	93.3(2)	N5$^{\#1}$-Zn1-O2W	89.7(2)
N3$^{\#1}$-Co-N1	91.8(15)	N2-Co-N1	81.0(2)	O1-Zn1-O2W	87.48(18)
------	------	N7-Co-N1	103.3(2)	O1$^{\#1}$-Zn1-O2W	92.52(18)
------	------	N3-Co-N1	161.5(2)	N5-Zn1-O2W$^{\#1}$	89.7(2)
------	------	N6-Co-N1	89.8(2)	N5$^{\#1}$-Zn1-O2W$^{\#1}$	90.3(2)
------	------	N2-Co-N8	105.9(2)	O1-Zn1-O2W$^{\#1}$	92.52(18)
------	------	N7-Co-N8	80.81(2)	O1$^{\#1}$-Zn1-O2W$^{\#1}$	87.48(18)
------	------	N3-Co-N8	88.5(2)	O2W-Zn1-O2W$^{\#1}$	180.0
------	------	N6-Co-N8	161.4(2)	N9-Zn2-N9$^{\#2}$	180.0
------	------	Zn1-N5	2.057(5)	N9-Zn2-O3	83.03(17)
------	------	Zn2-N9	2.075(6)	N9$^{\#2}$-Zn2-O3	96.97(17)
------	------	N9-Zn2-O3$^{\#2}$	96.96(17)	N9-Zn2-O1W$^{\#2}$	90.6(2)
------	------	N9$^{\#2}$-Zn2-O3$^{\#2}$	83.04(17)	N9$^{\#2}$-Zn2-O1W$^{\#2}$	89.4(2)
------	------	O3-Zn2-O3$^{\#2}$	179.997(1)	O3-Zn2-O1W$^{\#2}$	92.05(19)
------	------	O1W$^{\#2}$-Zn2-O1W	180.0	O3$^{\#2}$-Zn2-O1W$^{\#2}$	87.95(19)
------	------	O3-Zn2-O1W	87.95(19)	N9-Zn2-O1W	89.4(2)
------	------	O3$^{\#2}$-Zn2-O1W	92.05(19)	N9$^{\#2}$-Zn2-O1W	90.6(2)

[a]Symmetry operations (#) used to generate equivalent atoms: #1 = -x+1,-y,-z, #2 = -x+3/2,-y+1/2,-z+1/2

Table S2. Selected bond lengths (Å) and bond angles (°) for the HCP **3**.

Bond	**3**	**Bond**	**3**

Bond	**4**	Bond	**4**
Co1—N1	1.948(4)	N20—Cd	2.231(4)
Co1—N2	1.866(4)	N2-Co1-N1	81.73(17)
Co1—N3	1.939(4)	N2-Co1-N3	80.91(16)
Co1—N6	1.966(4)	N7-Co1-N6	82.05(17)
Co1—N7	1.867(4)	N7-Co1-N8	80.28(2)
Co1—N8	1.961(4)	N7-Co1-N2	176.57(17)
Co2—N11	1.962(4)	N1-Co1-N6	92.23(19)
Co2—N12	1.866(4)	N8-Co1-N3	88.68(16)
Co2—N13	1.967(4)	N17-Co2-N18	99.29(17)
Co2—N16	1.960(4)	N17-Co2-N16	81.90(2)
Co2—N17	1.866(4)	N12-Co2-N13	81.38(17)
Co2—N18	1.953(4)	N12-Co2-N11	80.44(18)
N4—Cd	2.233(4)	N17-Co2-N12	178.55(19)
N9—Cd	2.240(4)	N13-Co2-N16	94.54(19)
N15—Cd	2.241(4)	N11-Co2-N18	89.56(17)
Co1-N1	1.876(5)	N6-Co1-N4	96.3(3)

Table S3. Selected bond lengths (Å) and bond angles (°) for the HCP **4**.

Co1-N6	1.869(5)	N1-Co1-N9	101.0(2)
Co1-N4	1.957(5)	N6-Co1-N9	80.7(2)
Co1-N9	1.958(5)	N4-Co1-N9	89.4(2)
Co1-N7	1.958(5)	N1-Co1-N7	97.8(2)
Co1-N2	1.981(4)	N6-Co1-N7	80.5(2)
Hg-N10$^{\#1}$	2.235(6)	N4-Co1-N7	93.2(2)
Hg-N8	2.322(7)	N9-Co1-N7	161.2(2)
Hg-Cl	2.345(3)	N7-Co1-N2	90.5(2)
Hg-N5$^{\#1}$	2.652(7)	N10$^{\#1}$-Hg-N8	96.8(2)
Hg-N3	2.652(7)	N10$^{\#1}$-Hg-Cl	138.7(2)
Hg$^{\#2}$ -N5	2.235(6)	N8-Hg-Cl	123.8(17)
Hg$^{\#2}$-N10	2.235(6)	N10$^{\#1}$-Hg-N5$^{\#1}$	97.6(2)
N1-Co1-N6	176.4(2)	N8-Hg-N5$^{\#1}$	89.4(3)
N1-Co1-N4	80.7(2)	Cl-Hg-N5$^{\#1}$	90.6(17)

[a]Symmetry operations (#) used to generate equivalent atoms: #1= x,y,z-1 #2 = x,y,z+1.

Table S4: Crystallographic data collection and structural refinement parameters for **1-4**.

Compound	**1**	**2**	**3**	**4**
Formula	$NaC_{26}H_{22}CoN_{10}O_6S_4$	$C_{26}H_{22}ZnClCoN_{10}O_{10}S_4$	$C_{27}H_{26}CdClCoN_{10}O_9S_4$	$C_{26}H_{22}ClCoHgN_{10}O_4S_4$
Formula weight	780.70	922.59	969.60	961.79
T (K)	293(2)	293(2) K	100 (2)	293(2)
System	Orthorhombic	Monoclinic	Triclinic	Trigonal
Space group	*P c c n*	*I 2/a*	P -1	R-3
a (Å)	9.7473(9)	16.106(5)	9.488(6)	43.866
b (Å)	17.3697(15)	29.674(5)	12.563(8)	43.866
c (Å)	18.2266(18)	16.658(5)	16.137(9)	9.542
α (°)	90.0	90.0(5)	70.636(3)	90
β (°)	90.0	90.380(5)	86.729(3)	90
γ (°)	90.0	90.000(5)	89.399(2)	120
V ($Å^3$)	3085.9(5)	7961(4)	1811.7(19)	15899.3(11)
Z	4	8	2	18
ρ_{calc} (mg/m^3)	1.681	1.539	1.778	1.808
μ(mm^{-1})	0.902	1.358	1.414	5.169
F (000)	1592.0	3728	972	8424
Goodness of-fit (GOF) on F^2	1.082	1.013	1.090	0.910
Final R indices $[I>2\sigma(I)]$[a]	0.0657	0.0716	0.0426	0.0513
R indices (all data)	0.1101	0.1787	0.1160	0.1304

[a] $R1 = \Sigma||Fo| - |Fc||/\Sigma|Fo|$; $wR = \{\Sigma[w(Fo^2 - Fc^2)^2]/\Sigma[wFo^4]\}^{1/2}$.